IPNO-DRE. 94-21

EXPERIMENTAL SURVEY OF THE $(\vec{d},t)$ REACTION AT E_d = 200 MeV

J. VAN DE WIELE et al.
Institut de Physique Nucléaire
F-91406 Orsay, France

To be published in Phys. Rev. C

Experimental survey of the $(\vec{d},t)$ reaction at E_d=200 MeV

J. Van de Wiele[1], H. Langevin-Joliot[1], F. Jourdan[1],
J. Guillot[1], E. Gerlic[2], L. H. Rosier[1], A. Willis[1],
C. Djalali[1][3], M. Morlet[1], E. Tomasi-Gustafsson[4],
N. Blasi[5], S. Micheletti[5] and S. Y. van der Werf[6]

(1) Institut de Physique Nucléaire, IN2P3-CNRS, BP N°1 - 91406 Orsay, France

(2) Institut de Physique Nucléaire, IN2P3-CNRS, 43 Bd du 11 Novembre, 69622 Lyon-Villeurbanne, France

(3) Department of Physics and Astronomy, University of South Carolina, Columbia, South Carolina 29208

(4) DAPNIA-SPhN and Laboratoire National Saturne, CEN-Saclay, F 91191, Gif sur Yvette, France

(5) INFN and University of Milan, Physics Dept., Via Celoria 16, 20133 Milan, Italy

(6) Kernfysisch Versneller Instituut, 9747 AA Groningen, The Netherlands

(October 4, 1994)

Abstract

Differential cross sections, vector and tensor analyzing powers of the $(\vec{d},t)$ reaction on ^{120}Sn, ^{116}Sn, ^{90}Zr, ^{58}Ni, ^{16}O and ^{12}C have been measured at 200 MeV bombarding energy. Deuteron elastic scattering measurements have been performed on ^{116}Sn and ^{208}Pb at the same energy. These data have been analyzed together with previous ones on ^{58}Ni and ^{16}O to get best fit optical parameters describing deuteron elastic scattering. The $(\vec{d},t)$ experimental survey bears on 28 transitions populating well known valence levels, including previous data in ^{207}Pb and ^{27}Si. The vector and tensor analyzing powers exhibit striking similarities for transitions measured in different nuclei. The angular distributions are found to strongly depend on the number of nodes in the neutron form factor and on the coupling of spin and angular momentum $j_-=\ell-1/2$ versus $j_+=\ell+1/2$. The j effect is especially pronounced, for both analyzing powers for n=1 transitions. The slopes of the differential cross sections in different nuclei depend mainly on the number of nodes. Exact finite range calculations including S and D components have been performed, using two sets of deuteron parameters together with a deep triton potential. Both analyses reproduce rather well the differential cross sections and currently adopted spectrocopic factors. The conventional analyses with deuteron parameters fitting elastic scattering data reproduce rather well analyzing powers of $n>1$ transitions (with ℓ=0,1,2), but disagree with the data for n=1 transitions (except for j_+ A_{yy} values). Good or qualitative agreement is achieved for all transitions with the second deuteron potential, characterized by larger spin orbit terms and an additional imaginary tensor term. This allows using the reaction as a spectroscopic tool.

I. INTRODUCTION

Neutron inner hole response functions have been extensively studied for many years via transfer reactions, using unpolarized beams [1]. Angular distributions of vector analyzing powers A_y in $(\vec{p},d)$ and $(\vec{d},t)$ reactions have been successfully used in selected cases to get additional informations on the total spin j [1–3,5,6]. The method has been extended to the tensor analyzing powers A_{yy} in a recent study of ^{207}Pb inner hole states via the $(\vec{d},t)$ reaction at E_d=200 MeV [7]. A special interest of transfer reactions at intermediate energy comes from their strong selectivity in populating few high ℓ hole states, which are thus more easily disentangled among several overlapping subshells.

Both A_y and A_{yy} angular distributions of the four valence levels in ^{207}Pb most strongly populated via the $(\vec{d},t)$ reaction at E_d=200 MeV were shown in Ref. [8] to allow a clear identification of the pick-up transitions with $j_- = \ell - 1/2$ versus $j_+ = \ell + 1/2$. Exact finite range DWBA calculations reproduce rather well the corresponding observable σ, A_y and A_{yy} angular distributions. Large spin dependent terms in the deuteron potential were found necessary for describing the spin observables. It has seemed to us interesting to see if this conclusion and more generally the main features of the $(\vec{d},t)$ reaction mechanism as found on ^{208}Pb would be the same on other nuclei.

Nann et al. [9] have studied analyzing power angular distributions of the $(\vec{p},d)$ reaction at 94 MeV bombarding energy. They have found a distinctive j dependence for the pick-up of a neutron from $p_{1/2}$, $p_{3/2}$, $f_{5/2}$ and $f_{7/2}$ orbitals, which is rather independent of target mass and also of the number of nodes. The study of Hosono *et al.* [10] of the $(\vec{p},d)$ reaction at the lower incident energy of 65 MeV on nuclei ranging from ^{12}C to ^{94}Zr, points to a clear j dependence but also to a quite pronounced n dependence. No such systematic study of the $(\vec{d},t)$ reaction, even limited to σ and A_y observables, was available up to now.

We present in this paper an experimental survey of the $(\vec{d},t)$ reaction at E_d=200 MeV. The target nuclei are ^{208}Pb, ^{120}Sn, ^{116}Sn, ^{90}Zr, ^{58}Ni, ^{28}Si, ^{16}O and ^{12}C. The angular distributions measured for the cross section, the vector and tensor analyzing powers are compared with exact finite range DWBA predictions.

The measurements were done at forward angles, where pick-up cross sections are enhanced relative to those of multistep reactions responsible for a physical background at high excitation energies. This feature is most interesting for studying inner hole states. The data were complemented by a cursory investigation of deuteron elastic scattering on ^{208}Pb and ^{116}Sn.

The experimental procedure is described in sect. 2 and the data reduction in sect. 3. The experimental survey of the $(\vec{d},t)$ reaction at E_d=200 MeV and the discussion of angular distribution dependence on transition characteristics are the subject of sect. 4. DWBA analysis of the $(\vec{d},t)$ reaction data and analysis of elastic scattering are presented in sect. 5. Sect. 6 summarizes the results and conclusions.

II. EXPERIMENTAL PROCEDURE

We have used the polarized deuteron beam available at the Laboratoire National Saturne (LNS). Deuterons polarized in four different states called 5, 6, 7 and 8 [11] which are

linear combinations of vector and tensor polarization states, were accelerated sequentially in successive bursts.

The outgoing particles labelled with the corresponding deuteron polarized state were analyzed by the high resolution spectrometer SPES 1 working in the dispersion matching mode.

The first three localisation chambers of the polarimeter "POMME" were used to measure the trajectory positions and angles at the focal plane [12]. The "POMME" trigger allows in addition a measurement of energy loss and time of flight. No special selection of the tritons (or elastically scattered deuterons) was needed as background events were negligible.

Two scintillator telescopes, one in the reaction plane at -45°, the other in the vertical plane at 50° were used to continuously monitor the beam. Special care was taken in the choice of the threshold and high voltage conditions to achieve the best stability of the response. The counting rates of each telescope were averaged over the four polarization states. Except for the Mylar and CH_2 targets used for studying ^{16}O and ^{12}C, the two monitors were calibrated for each target by the carbon activation method used at the LNS [13]. A new calibration was also performed under the above conditions for the thick ^{208}Pb target used in our previous studies [8]. For spectrometer angles larger than 13.5°, the beam was focussed into a cavity of the shielding wall and stopped in a thick isolated aluminium block. This simplified Faraday cup was used to check the different target calibrations, which were found consistent except for the Zr target. The Faraday cup results were used for renormalizing the Zr calibration by a factor 1.20, and also for calibrating the Mylar and CH_2 targets. The cross sections calculated from the two monitor informations agreed within less than 10% (generally 5%), and statistical errors were generally very small. We adopted conservatively an uncertainty of 10% on cross sections at each angle (or the statistical errors if larger). An additional systematic error of $\sim$ 15% cannot be excluded on all cross-sections, taking into account uncertainties in the activation measurements.

The vector and tensor polarization parameters ρ_{10} and ρ_{20} of the deuteron beam were periodically measured with the low energy $d(\vec{d},p)t$ polarimeter [11]. They were found to be very stable at $\rho_{10} = -0.375 \pm 0.007$ and $\rho_{20} = 0.640 \pm 0.007$ which correspond to 92% and 90.5% of the maximum values of the vector and tensor polarization parameters. Calibration of the low energy polarimeter with dead time corrections may account for an additional 5% systematic errors on the deduced A_y and A_{yy} values from the relations:

$$A_y = \sqrt{\frac{2}{3}} \frac{1}{\mid \rho_{10} \mid} \frac{N_5 + N_7 - N_6 - N_8}{\sum_i N_i} \tag{2.1}$$

$$A_{yy} = \sqrt{2} \frac{1}{\mid \rho_{20} \mid} \frac{N_5 + N_6 - N_7 - N_8}{\sum_i N_i} \tag{2.2}$$

Here $N_{5,6,7,8}$ are the number of counts in each polarization state.

$$A_0 = (N_5 - N_6 - N_7 + N_8)/(\sum_i N_i)$$

which should vanish [11], was found to be equal to zero within 1 % assuming the same number of incident deuterons on the target for each polarization state.

The targets used in the present experiment were ^{120}Sn (99.6% enriched), ^{116}Sn (97.5% enriched),^{90}Zr (79% enriched), ^{58}Ni (natural), ^{16}O (mylar), ^{12}C (CH_2). The targets thicknesses were respectively 39.6 mg/cm^2 , 39.9 mg/cm^2, 40.0 mg/cm^2, 40.4 mg/cm^2, 10.45 mg/cm^2 and 8.55 mg/cm^2. ^{208}Pb [8] and ^{28}Si [14] were studied in a previous experiment. The choice of thick targets allowed a survey of the main excited state angular distributions within a short beam time. Under these conditions, the achieved energy resolution was typically 200 keV for all the targets. The " POMME" detection system together with a rather thick exit window of the spectrometer contribute for $\sim$ 80-100 keV to the overall energy resolution. The incident beam transport settings for the Mylar and CH_2 measurements were those optimized for the heavy targets, the main purpose being to check and subtract out ^{15}O and ^{11}C impurity peaks in residual heavy nucleus spectra. The energy resolution thus reached $\sim$ 300 keV at the largest angles.

The $(\vec{d},t)$ reaction measurements were performed at six or seven angular settings of the spectrometer from 3° to 18° or 22° except for the mylar and CH_2 target only studied up to 15°. The spectrometer entrance slits were set to achieve the maximum horizontal and vertical aperture angles of 2.4° and 4° respectively. The scattering angle was determined to better than 0.25° in reconstructing the trajectories. For each measurement, the horizontal acceptance was divided in two intervals of 1°.

The deuteron elastic scattering measurements were performed from 7° to 24° in 1° steps for ^{208}Pb and 2° steps for ^{116}Sn. The horizontal and vertical aperture angles were respectively 0.4° and 1°.

III. DATA REDUCTION

Excitation energies, number of nodes, orbital and total angular momentum $n\ell j$ of the levels studied in each nucleus are summarized in Table 1. These low-lying levels are in most cases rather pure single-hole states, and their spectroscopic factors are known from several experiments. The corresponding peaks measured in the present experiment are generally not well separated. A fitting procedure is thus needed to separate out the contributions of each reference level. For this purpose, the raw spectra of the number of counts measured for each of the polarized states 5, 6, 7 and 8 have been used to build the excitation energy spectra of independent observables, here σ, σA_y and σA_{yy}, following eqs. (2.1,2.2). The fits performed on these latter spectra give each individual level contribution and then the corresponding final values of σ, A_y andA_{yy}.

The fits were generally performed using as peak shape that of the well separated level at E_x=1.63 MeV in ^{207}Pb. The results did not change significantly for a 15% increase of the peak width. The position of the levels of interest were kept fixed, as their excitation energies are precisely known. Small global shifts of the energy scale (identical for the three observables) were allowed in order to achieve the best fit at each angle. The contributions of the other known levels with small cross sections or belonging to other residual nuclei than the one studied (^{90}Zr for the Zr target or $^{61,59}Ni$ for the Ni target) have been either subtracted out or taken into account in the fit. As discussed later on, we have used the ratio of such level spectroscopic factors over those of the reference levels with the same $n\ell j$, taken from the litterature, so that no new free parameter was necessary.

Fig. 1 shows a typical fit achieved for σ, σA_y and σA_{yy} observables in the case of ^{115}Sn residual nucleus at 5.5°. Note that a correction of a few percent corresponding to the estimated contribution of the $2d_{3/2}$ level at 0.5 MeV has been subtracted out of the experimental data. The fits including the $1g_{7/2}$, $1h_{11/2}$ and the first $2d_{5/2}$ levels are rather good.

Figs. 2 a,b,c show cross section spectra obtained for ^{119}Sn, ^{89}Zr and ^{57}Ni residual nuclei respectively, and the contributing peaks. In the case of ^{119}Sn, the group at E_x=1.35 MeV taken into account in the fit together with the $1h_{11/2}$, $1g_{7/2}$ and $2d_{5/2}$ reference levels and the small correction estimated for the $1/2^+$ and $3/2^+$ levels in the first peak are also shown (see Fig. 2a). The spectrum of Fig. 2b is somewhat more complex. In addition to the four levels of interest, the second $1g_{9/2}$ level at E_x=1.52 MeV in ^{89}Zr and the ^{90}Zr levels induced by the significant percentage of ^{91}Zr in the target have been taken into account. Their summed contribution is also shown in Fig. 2b. The relative spectroscopic factor of the E_x=1.52 MeV level was taken from Ref. [21]. The ^{90}Zr levels populated in the excitation energy region of interest are known as $(2d_{5/2} \otimes 1hole)$ multiplets [28,29]. The population of such levels via the (p,d) reaction at E_p=30 MeV has been compared in detail to that of the first ^{89}Zr valence hole levels in Ref. [28]. Further comparison has been performed with the same reaction at E_p=168 MeV up to higher excitation energy [30]. Relative ^{90}Zr level contributions in the $(\vec{d},t)$ observable spectra could thus be deduced confidently from these results. We have checked that even a 20% change of such contributions does not modify significantly the results, except for the $2p_{1/2}$ level. This has been taken into account in the error bars.

In the case of the ^{58}Ni target, we have used in the analysis the known positions of the levels in ^{59}Ni and ^{61}Ni and the ratio of their spectroscopic factors (see Refs. [31,32]), to those of the reference levels in ^{57}Ni. These contributions are negligible for the $1f_{7/2}$ levels as shown in Fig. 2c. The correction needed for the ^{57}Ni $1/2^-$ level is found too large for considering that level as a reference.

The angular distributions of the three observables σ, A_y and A_{yy} of each level are deduced respectively from the σ, σ A_y and σ A_{yy} fits. The corresponding errors take into account both fitting and statistical errors together with those on the polarization parameters.

IV. EXPERIMENTAL SURVEY OF THE $(\vec{d},t)$ REACTION

The differential cross sections measured in $^{119,115}Sn$, ^{89}Zr, ^{57}Ni, ^{27}Si, ^{15}O and ^{11}C are shown in Figs. 3-5. In heavy nuclei, their shapes are rather structureless, except for 2p states, and decrease nearly exponentially with angle. The structures are somewhat more pronounced in light nuclei. The slopes observed for transitions such as $1h_{11/2}$ and $1g_{7/2}$ in tin nuclei, or $1g_{9/2}$ and $1f_{5/2}$ in ^{89}Zr for example are nearly the same, while those for the $2d_{5/2}$ or $2p$ transitions are clearly much steeper. The same trend is observed in all other nuclei and has also been found in ^{207}Pb [8].

The vector and tensor analysing powers exhibit strong characteristic features, reminiscent of those observed in Ref. [8] for the $1i_{13/2}$, $1h_{9/2}$, $2f_{7/2}$ and $2f_{5/2}$ transitions in ^{207}Pb. Striking similarities among angular distributions measured for transitions in different nuclei lead us to classify them into four groups. The groups differ by the number of nodes n, and by the coupling of spin and orbital momentum $j_- = \ell - 1/2$ or $j_+ = \ell + 1/2$. It is worthwhile to

notice that the cross section angular distributions measured in different nuclei are also very similar if belonging to the same group (see Figs. 3-5).

The present classification of the transitions into four groups depending on j_+ versus j_- and on n is reminiscent of that given in Ref. [10] for the $(\vec{p},d)$ reaction at E_p=65 MeV.

1. j_+ transitions with n=1

As shown in Fig. 6-7, these transitions are characterized by negative vector analyzing powers. A_y reaches $\sim$ - 0.4 for all nuclei. The position of the minimum shifts only from $\sim$ 12° to $\sim$7° from ^{207}Pb to ^{11}C. Tensor analyzing powers exhibit a maximum around 12° increasing from typically $\sim$0.15 in ^{207}Pb to $\sim$0.35 in ^{15}O and ^{11}C.

2. j_- transitions with n=1

As shown in Fig. 6-7, both vector and tensor analyzing power characteristics strongly differ from those of the previous group. The vector analyzing powers are always positive and increase smoothly up to very large values as 0.6 - 0.8 . The tensor analyzing powers also increase up to $\sim$ 0.6, but they start from negative values $\sim$-0.4 near 0°. Transitions in light nuclei follow the general trend but with less smooth angular distributions.

3. j_+ transitions with n=2 or 3

In contrast to the j_+ transitions with n=1, the A_y values are in the present case positive, except at the smallest angles (see Fig. 8). Due to smaller cross sections, the errors are larger but anyway the similarities are clear for all nuclei. Tensor analyzing powers oscillate between $\sim$ -0.2 and $\sim$ 0.2. The n= 3 transition in ^{207}Pb does not show significantly different characteristics from n=2 transitions.

4. j_- transitions with n=2 or 3

These states are the most weakly populated in the present reaction. As only three transitions have be measured, no systematic behavior could be established from the angular distributions shown in Fig. 9. Also shown in Fig. 9, the ℓ =0 transition in ^{27}Si exhibits strongly oscillating features for both analyzing powers.

V. DWBA ANALYSIS OF THE $(\vec{d},t)$ REACTION

Finite range calculations have been performed with the code DWUCK5 [33], using range functions deduced in Ref. [34] with the Super Soft Core potential [35]. Both the S and D components of the range function are included. The target form factors are calculated in a Wood Saxon well with r=1.22 $A^{1/3}$ fm, a=0.7 fm, following predictions by Mahaux et al. [36] for ^{207}Pb with a spin-orbit strength parameter λ=27.5 .

It has been shown in Ref. [8] that the observable angular distributions of the $^{208}Pb(\vec{d},t)^{207}Pb$ reaction could not be reproduced with deuteron and triton potentials describing respectively elastic scattering on ^{58}Ni [37] and ^{3}He scattering on medium heavy targets [38]. On the other hand a very good agreement has been achieved for the $1i_{13/2}$, $1h_{9/2}$, $2f_{7/2}$ and $2f_{5/2}$ valence transitions using a modified deuteron potential and a rather deep triton potential derived under a very simplified adiabatic approach. The angular distributions of the many transitions selected in the present survey were first calculated using these last potentials. An overall fair agreement was already achieved with the data (except for the lightest nuclei). Optimisation of a few optical potential parameters leads, as discussed later on, to the parameter set D200D-T200 (see table II). On the other hand, the reanalysis of the deuteron elastic scattering data of Ref. [37] on ^{58}Ni and ^{16}O nuclei and the analysis of the new data on ^{208}Pb and ^{116}Sn allow the determination of elastic scattering parameter sets D200E, as summarized in table II.

The final calculations performed with potentials D200D-T200 and D200E-T200 are compared with the experimental results in Figs 3-9.

A. D200E deuteron elastic scattering optical potential

The elastic scattering angular distributions of the cross section and analyzing powers measured for ^{208}Pb and ^{116}Sn are shown in Fig. 10. The three observable data have been fitted with the program SEARCH [39], using initial parameters given for ^{58}Ni in Ref. [37], with a complex instead of a real spin orbit potential. Additional imaginary tensor terms, also first included in the search, converge toward very small values and were dropped. The data of Ref. [37] on ^{58}Ni and ^{16}O have been reanalyzed under the same conditions. The best fit parameters deduced for ^{16}O, ^{58}Ni, ^{116}Sn and ^{208}Pb are summarized in Table 2 (set D200E). The three observable angular distributions calculated with the best fit parameters describe the data very well.

B. D200D and T200 optical potentials

The $(\vec{d},t)$ differential cross sections depend mostly on the exit channel potential. For the medium mass and especially for the light nuclei, we have found it necessary to increase the depth of the triton real central potential given in Ref. [8], in order to better reproduce the angular distribution shapes, as illustrated in Figs. 3-4 for ^{115}Sn and ^{57}Ni transitions. The larger depths also reproduce better the rather well known spectroscopic factors and improve the description of vector analyzing powers for n=1 transitions (see Figs. 6-7). Such deeper potentials reduce the contribution of low ℓ partial wave amplitudes in the internal region of the nucleus.

The parameters of the deuteron central potential have relatively small effects on analyzing powers, as previously noted in Ref. [8]. They were kept the same as in Ref. [8] for all nuclei. On the other hand the calculated analyzing powers beyond $\sim 8^{\circ}$ depend strongly on the spin part of the deuteron potential and much less on the triton spin orbit potential. The parameter set D200D (see Table II) which achieves the best agreement in this respect, includes larger real and imaginary spin orbit terms as compared with the set D200E, together

with an additional tensor imaginary term. Such terms are found larger for light than for heavy targets

It is worthwhile to notice that the differential cross sections calculated with deuteron potential D200D reproduce the ^{208}Pb and ^{116}Sn elastic scattering differential cross sections rather well as shown in Fig. 10. On the other hand, the vector and especially the tensor analyzing powers calculated with that same potential exhibit significant discrepencies with the experimental results . We attempted to improve the description of both the elastic scattering and the pick-up data with a same deuteron potential by adding a non local central term depending on the momentum [40]. Such attempts performed with different geometries of the non local term were unsuccessful.

C. Comparison of experimental results and DWBA calculations

1. Differential cross sections and spectroscopic fators

The differential cross section shapes are generally rather well reproduced using D200D or D200E deuteron potentials, except in the lightest nuclei where D200D is needed to achieve a reasonable agreement (see Figs.3-5). It is worthwhile to notice that the shapes calculated for inner hole states with different ℓ values, are similar to those of the valence states belonging to the same n ,$j_{+/-}$ groups, as previously noted in Ref. [8]. This remark, together with the valence state results, leads to the conclusion that cross section angular distributions of the $(\vec{d},t)$ reaction at E_d=200 MeV are nearly independent both of ℓ and target mass. They depend mainly on the number of nodes and slightly on the spin orbit coupling.

The spectroscopic factors deduced from the present analysis with parameter sets D200E-T200 and D200D-T200 are compared in Table 1 with those currently adopted. The results do not differ significantly for the two sets of deuteron parameters, and agreement with adopted values is generally quite good, except in the lightest nuclei. The extracted C^2S values would decrease typically by less than $\sim$10% for target form factors calculated in a standard geometry well (r=1.25 fm). The values would also change by typically $\sim$10% if using range functions calculated with other nucleon-nucleon potentials.

2. Analyzing powers of j_+, n=1 transitions

As shown in Figs. 6-7, the experimental tensor analyzing powers are well or fairly well reproduced using D200D or D200E deuteron potentials. The characteristic behavior of A_y angular distributions is only well accounted for with the parameter set D200D beyond 8°, while a good agreement is achieved with the two potentials at forward angles.

3. Analyzing powers of j_-, n=1 transitions

Calculations with potentials D200D reproduce strikingly well both vector and tensor analyzing powers for heavy and medium mass nuclei, while potential D200E calculations exhibit strong discrepancies with the data (see Figs. 6 -7) . Potential D200D also achieves a better qualitative description of analyzing power angular distributions in light nuclei.

4. Analyzing powers of j_+ transitions with n=2,3

As shown in Fig. (8) a qualitative agreement with the data is achieved with both potentials. The analyzing powers of $2p_{3/2}$ transitions and the tensor analyzing power of the $3p_{3/2}$ transition in ^{207}Pb are however better reproduced with potential D200E.

5. Analyzing powers of j_- transitions with n=2,3

The main features of the vector analyzing powers are reproduced with the two potentials (see Fig. 9). This is also the case for the tensor analyzing power of the $2p_{1/2}$ transition in ^{89}Zr, while the $2f_{5/2}$ transition in ^{207}Pb is well reproduced only with potential D200D. The ℓ=0 $2s_{1/2}$ transition in ^{27}Si, in spite of being strongly mismatched, is quite well reproduced with potential D200D.

6. Effect of the D component in the range function

Calculations of the $(\vec{d},t)$ reaction on ^{116}Sn, ^{58}Ni and ^{16}O have been performed with parameter sets D200D-T200,but including the S component of the range function only. The shapes of the cross section and of the vector analyzing power angular distributions are nearly identical to those obtained with both S and D components. Exemples of tensor analyzing power angular distributions calculated with and without the D component are compared with the data in Fig. 11. In agreement with Ref. [8], the effect of the D component is systematically quite important at the most forward angles for j_- transitions with n=1, where it explains the large negative values observed toward 0°. A_{yy} decreases to a lesser extent, in that same angular region, for the transitions belonging to other groups. It is interesting to notice that the effect of the D component is negligeable beyond ~10° for the rather well matched transitions in heavy nuclei (see Fig. 11), as already observed in the case of ^{207}Pb [8]. On the other hand, significant effects are observed beyond ~ 8° for the transitions in lighter nuclei. In agreement with the results on ^{207}Pb [8], the absolute cross sections calculated in all nuclei with the S component only, are smaller than with S and D components. This decrease may reach typically 20% for j_- transitions with n=1.

VI. SUMMARY AND CONCLUSIONS

The present work is the first systematic survey of the $(\vec{d},t)$ reaction performed at intermediate energy. Differential cross sections, vector and tensor analyzing powers of the most populated valence states have been measured on target nuclei from ^{12}C to ^{120}Sn at 200 MeV bombarding energy. Results on the $^{208}Pb(\vec{d},t)^{207}Pb$ [8] at the same incident energy are included in the discussion. Previous measurements on deuteron elastic scattering at E_d=200 MeV [37] have been complemented for heavy targets.

The experimental survey bearing on 28 transitions leads to the main following conclusions.

The angular distribution shapes of all three observables are rather independent of target mass. The differential cross sections are rather structureless and their slopes depend mainly

of the number of nodes n in the neutron form factor, and slightly on j_+ versus j_-. On the other hand, the A_y and A_{yy} angular distributions exhibit j_+ versus j_- effects and a dependence on n. The j signature is especially pronounced, for both vector and tensor analyzing powers, for the transitions with n=1. As compared with the behavior of the $(\vec{p},d)$ reaction at E_p=65 (Ref. [10]) and 94 MeV (Ref. [9]), the $(\vec{d},t)$ reaction at E_d=200 MeV presents most interesting features at forward angles for the best matched n=1 transitions. The associated A_y observables for j_+ and j_- transitions have then systematically opposite signs.

The experimental results have been compared with exact finite range DWBA calculations, using S and D components of the range function. The differential cross sections are rather well described using deuteron potentials fitting elastic scattering and deep triton potentials. A_y and A_{yy} angular distributions for transitions with n larger than 1 (and ℓ=0,1,2) are also generally well or fairly well reproduced. The vector and tensor analyzing powers of n=1 transitions are also well reproduced below $\sim$10°. At larger angles, the calculations exhibit significant discrepancies, especially with the vector analyzing power data of j_+ transitions and the tensor analyzing power data of j_- transitions. It is striking that a satisfactory description can however be achieved for all three observables σ, A_y and A_{yy} for all nuclei (even qualitatively for the lightest ones), using a modified deuteron potential. That potential is characterized by larger spin orbit terms and additional imaginary tensor term as already successfully used for ^{207}Pb [8]. The spectroscopic factors deduced for all studied transitions with both sets of deuteron parameters are similar, agreement with adopted values from previous works beeing generally quite good.

We emphasize that the above description of the $(\vec{d},t)$ reaction at E_d=200 MeV is especially successful for the highest ℓ transitions which dominate residual excitation energy spectra in heavy or medium heavy nuclei. The present survey confirms the reaction as a good spectroscopic tool for studying inner hole state fragmentation and spreading in such nuclei.

ACKNOWLEDGMENTS

We are very grateful to Y. Bisson, G. Chesneau and R. Margaria for their efficient help in the technical support before and during the experiment. The technical staff of the Laboratoire National Saturne is acknowledged for its assistance during the experiment. One of the authors (C.D.) was supported by a grant from the U.S Department of Energy and the National Science Foundation.

REFERENCES

[1] S. Galès, Ch. Stoyanov and A.I Vdovin, Physics Reports **166**, 125 (1988) and references therein.

[2] G.M. Crawley, J. Kasagi, S. Galès, E. Gerlic, D. Friesel and A. Bacher, Phys. Rev. **C23**, 1818 (1981).
J. Kasagi, G.M. Crawley, E. Kashy, J. Duffy, S. Galès, E. Gerlic and D. Friesel, Phys. Rev. **C28**, 1065 (1983).

[3] G. Perrin, G. Duhamel, C. Perrin, E. Gerlic, S. Galès and V. Comparat, Nucl. Phys. **A356**, 61 (1981).

[4] S.Galès, E . Gerlic, G . Duhamel, G . Perrin, C . Perrin and V . Comparat, Nucl. Phys. **A381**, 40 (1982).

[5] R. H. Siemssen, C. C. Foster, W. W. Jacobs, W. P. Jones, D. W. Miller, M. Saber and F. Soga, Nucl. Phys. **A405**, 205 (1983).

[6] G. Duhamel-Chretien, G. Perrin, C. Perrin, V. Comparat, E. Gerlic, S. Galès and C. P. Massolo, Phys. Rev. **C43**, 1116 (1991).

[7] H. Langevin-Joliot, J. Van de Wiele, J. Guillot, E. Gerlic, L. H. Rosier, A. Willis, M. Morlet, G. Duhamel-Chretien, E. Tomasi-Gustafsson, N. Blasi, S. Micheletti and S. Y. van der Werf, Phys. Rev. **C47**, 1571 (1993).

[8] J. Van de Wiele, H. Langevin-Joliot, J. Guillot, L. H. Rosier, A. Willis, M. Morlet, G. Duhamel-Chrétien, E. Gerlic, E. Tomasi-Gustafsson, N. Blasi, S. Micheletti and S. van der Werf, Phys. Rev. **C46**, 1863 (1992).

[9] H. Nann, D. W. Miller, W. W. Jacobs, D. W. Devins, W. P. Jones and Li Qing-Li, Phys. Rev. **C27** 1073 (1983).

[10] K. Hosono, M. Kondo, T. Saito, N. Matsuoka, N. Nagamachi, T. Noro, H. Shimizu, S. Kato, K. Okada, K. Ogino and Y. Kadota, Nucl. Phys. **A343**, 234 (1980).

[11] J. Arvieux, S.D. Baker, A. Boudard, J. Cameron, T. Hasegawa, D. Hutcheon, C. Kerboul, G. Gaillard and Nguyen Van Sen, Nucl. Instrum. and Methods. **A273**, 48 (1988).

[12] B. Bonin, A. Boudard, H. Fanet, R. W. Fergerson, M. Garçon, C. Giorgetti, J. Habault, J. Le Meur, R. M. Lombard, J. C. Lugol, B. Mayer, J. P. Mouly, E. Tomasi-Gustafsson, J. C. Duchazeaubeneix, J. Yonnet, M. Morlet, J. Van de Wiele, A. Willis, G. Greeniaus, G. Gaillard, P. Markowitz, C. F. Perdrisat, R. Abegg, and D. A. Hutcheon, Nucl. Instrum. Methods **A288**, 379(1990).

[13] H. Quechon, Thesis Orsay, 1980. J. Radin, H. Quechon, G.M. Raisbeck and F. Yiou, Phys. Rev. **C26**, 2565 (1982).

[14] F . Jourdan, J. Van de Wiele, G . Duhamel, E . Gerlic, J . Guillot, H . Langevin-Joliot, M . Morlet, L .H . Rosier, A . Willis, IPN-DRE Orsay Annual Report, 99 (1990).

[15] P. G. Roos, S. M. Smith, V. K. C. Chenz, G. Tibell, A. A. Cowley, and R. A. J. Riddle, Nucl. Phys. **A255**, 187 (1975).

[16] D. Karban, A. K. Basak, J. B. A. England, G. C. Morrison, J. M. Nelson, S. Roman, and G. G. Shute, Nucl. Phys. **A269**, 312 (1976).

[17] B. M. Preedom, Phys. Rev. **C5**, 587 (1972).

[18] G. D. Jones, R. R. Johnson and R. J. Griffiths, Nucl. Phys. **A107**, 653 (1968).

[19] R. L. Kozub, Phys. Rev. **172**, 1078 (1968).

[20] S.Fortier and S. Galès, Nucl. Phys. **A321**, 137 (1979).

[21] S.Galès, E. Hourani, S. Fortier, H. Laurent, J. M. Maison and J. P. Schapira., Nucl. Phys. **A288**, 221 (1977).
[22] E. Gerlic, G. Berrier-Ronsin, D. Duhamel, S. Galès, E. Hourani, H. Langevin-Joliot, M. Vergnes, and J. Van de Wiele, Phys. Rev. **C21**, 24 (1980).
[23] S. A. Dickey, J. J. Kraushaar, R. A. Ristiner, M. A. Rumore, Nucl. Phys. **A377**, 137 (1982).
[24] J. Guillot, J. Van de Wiele, H. Langevin-Joliot, E. Gerlic, J. P. Didelez, G. Duhamel, G. Perrin, M. Buenerd, and J. Chauvin, Phys. Rev. **C21**, 879 (1980).
[25] S. Galès, G. M. Crawley, D. Weber and B. Zwieglinski, Phys. Rev. **C18**, 2475 (1978).
[26] S. M. Smith, P. G. Roos, C. Moazed and A. M. Bernstein, Nucl. Phys. **A173**, 32 (1971).
[27] W. A. Lanford and G. M. Crawley, Phys. Rev. **C9** 646 (1974).
[28] J. B. Ball and C. B. Fulmer, Phys. Rev. **172**,1199 (1968).
[29] H. Fann J. P. Schiffer and U. Strohbusch, Phys. Letts. **44B**, 19 (1973).
[30] G. Duhamel, E. Gerlic, J. Guillot, H. Langevin-Joliot, G. Perrin, A. Taleb, J. Van de Wiele, IPN-DRE Orsay Annual Report, 62 (1986).
[31] W. R. Zimmerman, J. J. Kraushaar, M. J. Schneider and H. Rudolph, Nucl. Phys. **A297**, 263 (1978).
[32] D. H. Koang, W. S. Chien and H. Rossner, Phys. Rev. **C13**, 1470 (1976).
[33] DWUCK5, P. D. Kunz, University of Colorado, Boulder, CO80309.
[34] J. L. Ballot, J. Van de Wiele, G. Cory to be submitted for publication. J. Van de Wiele, IPN-DRE Orsay Annual Report, 78 (1989).
[35] R. De Tourreil et D. W. Sprung, Nucl. Phys. **A201**, 193 (1973).
[36] C. Mahaux and R. Sartor, Nucl. Phys. **A493**, 157 (1989) and references therein.
[37] Nguyen Van Sen, J. Arvieux, Ye Yanlin, G. Gaillard, B. Bonin, A. Boudard, G. Bruge, J. C. Lugol, R. Babinet, T. Hasegawa, F. Soga, J. M. Cameron, G. C. Neilson and D. M. Sheppard, Phys. Lett. **156B**, 185 (1985).
[38] N. Willis, I. Brissaud, Y. Le Bornec, B. Tatischeff, and G. Duhamel, Nucl. Phys. **A204**, 454 (1973).
[39] J. Van de Wiele and A. Willis, Code SEARCH, unpublished (1993).
[40] J. Van de Wiele and F. Jourdan, IPNO-DRE 94.08, Orsay (1994).

FIGURES

FIG. 1. Typical fits of σ, σ A_y and σ A_{yy} ^{115}Sn excitation energy spectra taken at 5.5°. Solid lines: Experimental spectra, corrected for the small contribution of the $3/2^+$ level at 0.5 MeV. Stars: Best fit spectra. Other lines: $1g_{7/2}$, $1h_{11/2}$ and $2d_{5/2}$ components.

FIG. 2. Decomposition of the ^{119}Sn, ^{89}Zr and ^{57}Ni excitation energy spectra taken at 5.5° into the reference level peaks, and impurity or secondary peak contributions. Solid lines: Experimental spectra. Dashed lines: Peaks corresponding to the reference levels listed in Table I. Dotted lines: Other peaks. (a) ^{119}Sn. Hatched area: Subtracted contribution of the $1/2^+$ (0.0 MeV) and $3/2^+$ (0.029 MeV) levels. (b). ^{89}Zr. Hatched area: Summed contributions of the ^{90}Zr excited levels and of the ^{89}Zr level at E_x=1.52 MeV (see text). (c) ^{57}Ni. Hatched area: Contribution of the heavier nickel isotopes below 3 MeV and beyond 5 MeV.

FIG. 3. $^{120,116}Sn(\vec{d},t)^{119,115}Sn$ differential cross sections at E_d=200 MeV. Solid lines : Finite range calculations with S and D components and optical parameter set D200D-T200. Dashed lines : The same with parameter set D200E-T200. Dotted lines: Calculation with parameter set D200D and V_t=-98.3 MeV for ^{115}Sn.

FIG. 4. $^{90}Zr(\vec{d},t)^{89}Zr$ and $^{58}Ni(\vec{d},t)^{57}Ni$ differential cross sections at E_d=200 MeV. The two $1f_{7/2}$ levels in ^{57}Ni indicated (a) and (b) are respectively the $T_<$ level at E_x=2.57 MeV and the $T_>$ level at E_x=5.25 MeV. Solid and dashed lines as in Fig. 3. Dotted lines: same as Fig. 3, but for ^{57}Ni residual nucleus.

FIG. 5. Differential cross sections of the $(\vec{d},t)$ reaction populating ^{27}Si, ^{15}O and ^{11}C residual nuclei. Solid and dashed lines as in Fig. 3.

FIG. 6. A_y and A_{yy} angular distributions for j_+ and j_- transitions with $n = 1$, in heavy nuclei. Solid, dashed and dotted lines as in Fig. 3.

FIG. 7. A_y and A_{yy} angular distributions for j_+ and j_- transitions with $n = 1$, in medium mass and light nuclei. Solid, dashed and dotted lines as in Fig. 4.

FIG. 8. A_y and A_{yy} angular distributions for j_+ transitions with n=2 or 3. Solid and dashed lines as in Fig. 3. Dotted lines: The same as in Fig. 3 for ^{115}Sn and Fig. 4 for ^{57}Ni

FIG. 9. A_y and A_{yy} angular distributions for j_- transitions with n=2 or 3, and the $2s_{1/2}$ transition in ^{27}Si. Solid and dashed lines as in Fig. 3.

FIG. 10. σ, A_y and A_{yy} angular distributions of elastically scattered deuterons at E_d=200 MeV on ^{208}Pb and ^{116}Sn target nuclei. Solid lines: Calculation with potential parameters D200D (see Table II and text). Dashed Lines: Calculation with the best fit potential parameters D200E given in Table II.

FIG. 11. Dependence of A_{yy} angular distributions on the S and D components of the Range function . Left: j_+ n=1 transitions. Right: j_- n=1 transitions. Solid lines: Calculations with S and D components. Dashed lines: S component only.

TABLES

TABLE I. Characteristics of the reference level transitions. The spectroscopic factors deduced with deuteron potentials D200D and D200E are compared with typical results from previous works.

Residual Nucleus	E_x MeV	J^π	nlj	C^2S Other Works		C^2S D200D	C^2S D200E
^{11}C	0.	$3/2^-$	$1p_{3/2}$	2.5[a]	3.06[b]	5.2	4.2
	2.	$1/2^-$	$1p_{1/2}$	0.6[a]	0.7[b]	(0.9)	(0.8)
^{15}O	0.	$1/2^-$	$1p_{1/2}$	2.4[a]	2.2[c]	2.8	3.2
	6.18	$3/2^-$	$1p_{3/2}$	3.4[a]	4.3[c]	5.0	5.1
^{27}Si	0.	$5/2^+$	$1d_{5/2}$	2.1[d]	3.5[e]	3.8	3.9
	0.78	$1/2^+$	$2s_{1/2}$	0.65[d]	0.65[e]	(0.4)	(0.5)
	0.96	$3/2^+$	$1d_{3/2}$	0.37[d]	0.35[e]	(0.3)	(0.35)
	4.13	$1/2^-$	$1p_{1/2}$		1.2[e]	1.1	1.4
^{57}Ni	0.	$3/2^-$	$2p_{3/2}$	1.05[f]	1.0[g]	1.3	1.3
	0.76	$5/2^-$	$1f_{5/2}$	1.05[f]	0.63[g]	0.9	1.0
	2.57	$7/2^-$	$1f_{7/2}$	3.1[f]	1.91[g]	3.1	3.0
	5.25	$7/2^-$	$1f_{7/2}(T_>)$	2.05[f]	1.08[g]	2.3	2.2
^{89}Zr	0.	$9/2^+$	$1g_{9/2}$	8.0[h]	7.1[i]	8.2	7.6
	0.59	$1/2^-$	$2p_{1/2}$	1.7[h]	2.4[i]	1.9	2.0
	1.09	$3/2^-$	$2p_{3/2}$	2.5[h]	2.7[i]	3.5	3.2
	1.45	$5/2^-$	$1f_{5/2}$	2.5[h]	3.0	2.1	2.2
^{115}Sn	0.614	$7/2^+$	$1g_{7/2}$	7.5[j]	5.0[k]	6.5	6.5
	0.714	$11/2^-$	$1h_{11/2}$	2.0[j]	1.5[k]	2.2	2.0
	0.985	$5/2^+$	$2d_{5/2}$	4.7[j]	3.9[k]	5.1	4.8
^{119}Sn	0.089	$11/2^-$	$1h_{11/2}$	3.5[j]	3.30[l]	4.6	4.2
	0.788	$7/2^+$	$1g_{7/2}$	6.0[j]	5.15[l]	7.0	7.0
	1.09	$5/2^+$	$2d_{5/2}$	2.6[j]	2.85[l]	4.5	4.2
^{207}Pb	0.0	$1/2^-$	$3p_{1/2}$	2.0[m]	1.6[n]	(1.8)	(1.6)
	0.57	$5/2^-$	$2f_{5/2}$	5.5[m]	3.8[n]	3.7	3.3
	0.90	$3/2^-$	$3p_{3/2}$	4.9[m]	4.6[n]	(4.1)	(3.6)
	1.63	$13/2^+$	$1i_{13/2}$	10.2[m]	12.1[n]	10.3	8.8
	2.34	$7/2^-$	$2f_{7/2}$	5.7[m]	6.7[n]	5.3	4.9
	3.42	$9/2^-$	$1h_{9/2}$	5.9[m]	4.85[n]	4.3	4.3

[a] Ref. [15].

[b] Ref. [16].

[c] Mean value from Ref. [17].

[d] Ref. [18].
[e] Ref. [19].
[f] Ref. [20].
[g] Mean value from Ref. [10].
[h] Ref. [21].
[i] Ref. [6].
[j] Ref. [22].
[k] Ref. [3].
[l] Ref. [23].
[m] Mean value from Ref. [24–27].
[n] Values deduced in Ref. [8] using the Paris potential for the range function, normalized by a factor 1.2 taking into account the revized target calibration.

TABLE II. Deuteron and triton optical potentials.

	V MeV	R_V fm	A_V fm	W MeV	R_W fm	A_W fm	V_{ls} MeV	R_{vls} fm	A_{Vls} fm	W_{ls} MeV	R_{Wls} fm	A_{Wls} fm
D200E												
^{16}O	-39.9	1.24	0.85	-15.5	1.47	0.78	-7.15	1.00	0.65	1.35	1.01	0.47
^{58}Ni	-41.1	"	0.82	-13.2	1.44	0.73	-6.55	1.08	0.69	1.95	1.02	0.47
^{116}Sn	-41.1	"	0.82	-14.3	1.38	0.81	-5.5	1.15	0.70	1.40	1.04	0.55
^{208}Pb	-41.2	"	0.83	-14.4	1.33	0.88	-5.4	1.14	0.73	0.90	1.05	0.63
D200D	-36.6	1.24	0.82	-13.3	1.45	0.69	-7.8	1.08	0.77	2.0[a] 4.0[b]	1.2	0.6
T200	$-V_t$[c]	1.19[d]	0.70	-18.5	1.52	0.68	-8.23	1.04	0.67	0.35	1.02	0.62

a) for ^{208}Pb,$^{120,116}Sn$ and ^{90}Zr.
b) for ^{58}Ni,^{28}Si, ^{16}O and ^{12}C.
c) V is 98.3 MeV for ^{207}Pb, 115 MeV for $^{119,115}Sn$, 130 MeV for ^{89}Zr and ^{57}Ni, and 160 MeV for ^{27}Si,^{15}O and ^{11}C residual nuclei.
d) for ^{207}Pb, 1.14 as in Ref. [8].

$$V_{opt}(r) = V\ f(x_v) + iW\ f(x_w) - \left[V_{ls}\ \frac{1}{r}\frac{d}{dr}f(x_{vls}) + iW_{ls}\ \frac{1}{r}\frac{d}{dr}f(x_{wls})\right]\mathbf{L}\cdot\mathbf{S}$$
$$+iW_{ts}f'(x_{wts})T_0^0(\mathbf{L},\mathbf{S})$$

$$\text{with } x_n = \frac{r - R_n}{A_n}\ f(x) = \frac{1}{1+e^x};\ f'(x) = \frac{d}{dx}f(x)$$

$$T_0^0(\mathbf{L},\mathbf{S}) = \begin{cases} (\mathbf{L}\cdot\mathbf{S})^2 + \frac{1}{2}\mathbf{L}\cdot\mathbf{S} - \frac{2}{3}\mathbf{L}^2 & \text{if } S = 1 \\ 0 & \text{if } S \leq \frac{1}{2} \end{cases}$$

For D200D, W_{ts}= -0.035[a] MeV, -0.07[b] MeV R_{ts}=1.1 fm A_{ts}=0.6 fm
For D200E, W_{ts}=0.

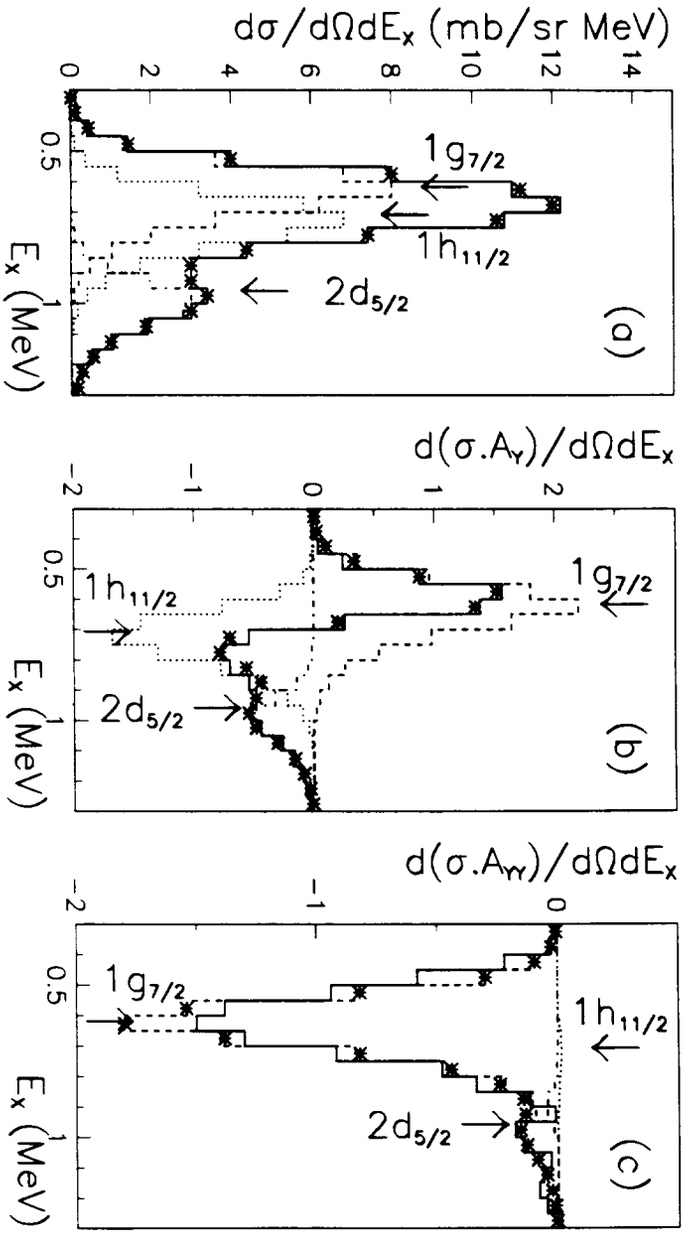
dσ/dΩdE$_x$ (mb/sr MeV)
0
2
4
6
8
10
12
14
0.5
1
E$_x$ (MeV)
1g$_{7/2}$
1h$_{11/2}$
2d$_{5/2}$
(a)
d(σ.A$_Y$)/dΩdE$_x$
−2
−1
0
1
2
0.5
1
E$_x$ (MeV)
1h$_{11/2}$
1g$_{7/2}$
2d$_{5/2}$
(b)
d(σ.A$_{YY}$)/dΩdE$_x$
−2
−1
0
0.5
1
E$_x$ (MeV)
1g$_{7/2}$
1h$_{11/2}$
2d$_{5/2}$
(c)

Fig. 1

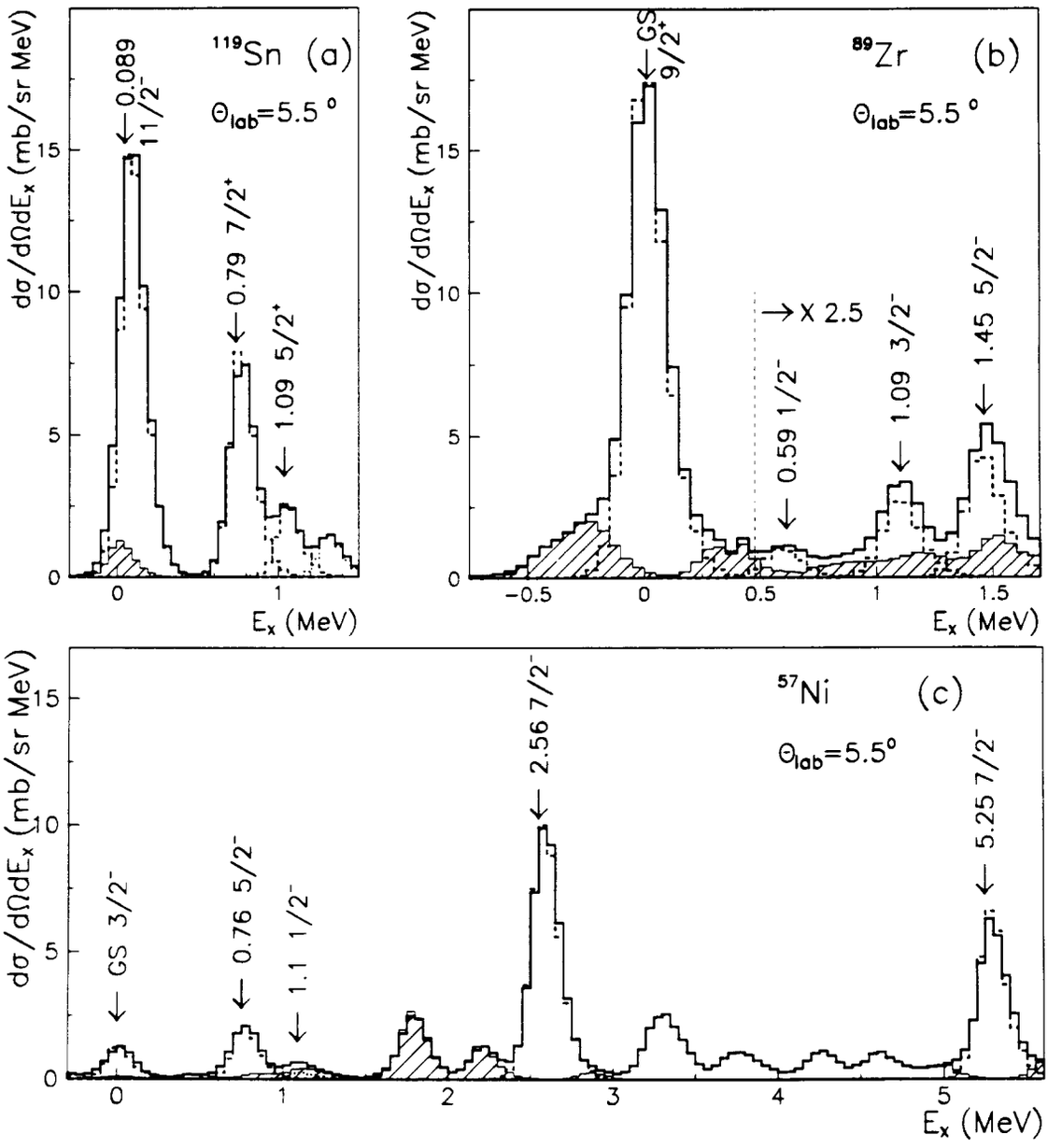
^{119}Sn (a)
Θ_{lab}=5.5 °
0.089 11/2$^-$
0.79 7/2$^+$
1.09 5/2$^+$
^{89}Zr (b)
Θ_{lab}=5.5 °
GS 9/2$^+$
X 2.5
0.59 1/2$^-$
1.09 3/2$^-$
1.45 5/2$^-$
^{57}Ni (c)
Θ_{lab}=5.5°
GS 3/2$^-$
0.76 5/2$^-$
1.1 1/2$^-$
2.56 7/2$^-$
5.25 7/2$^-$
dσ/dΩdE$_x$ (mb/sr MeV)
E$_x$ (MeV)

Fig. 2

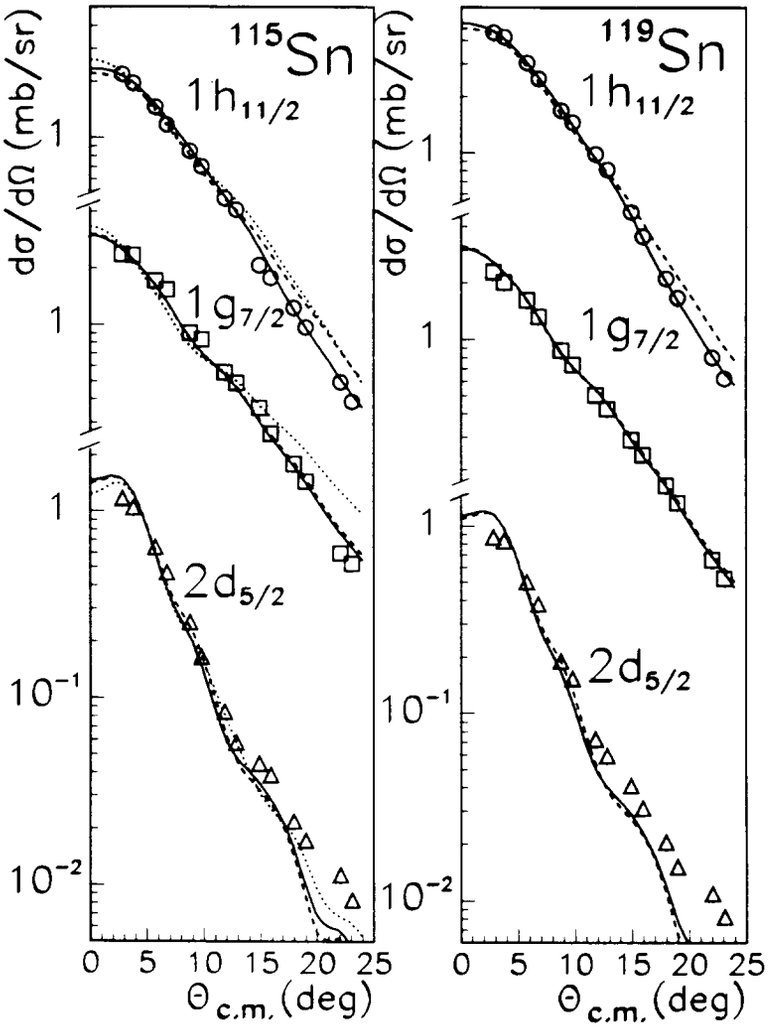
^{115}Sn
^{119}Sn
$1h_{11/2}$
$1g_{7/2}$
$2d_{5/2}$
dσ/dΩ (mb/sr)
1
10^{-1}
10^{-2}
0 5 10 15 20 25
$\Theta_{c.m.}$ (deg)

Fig. 3

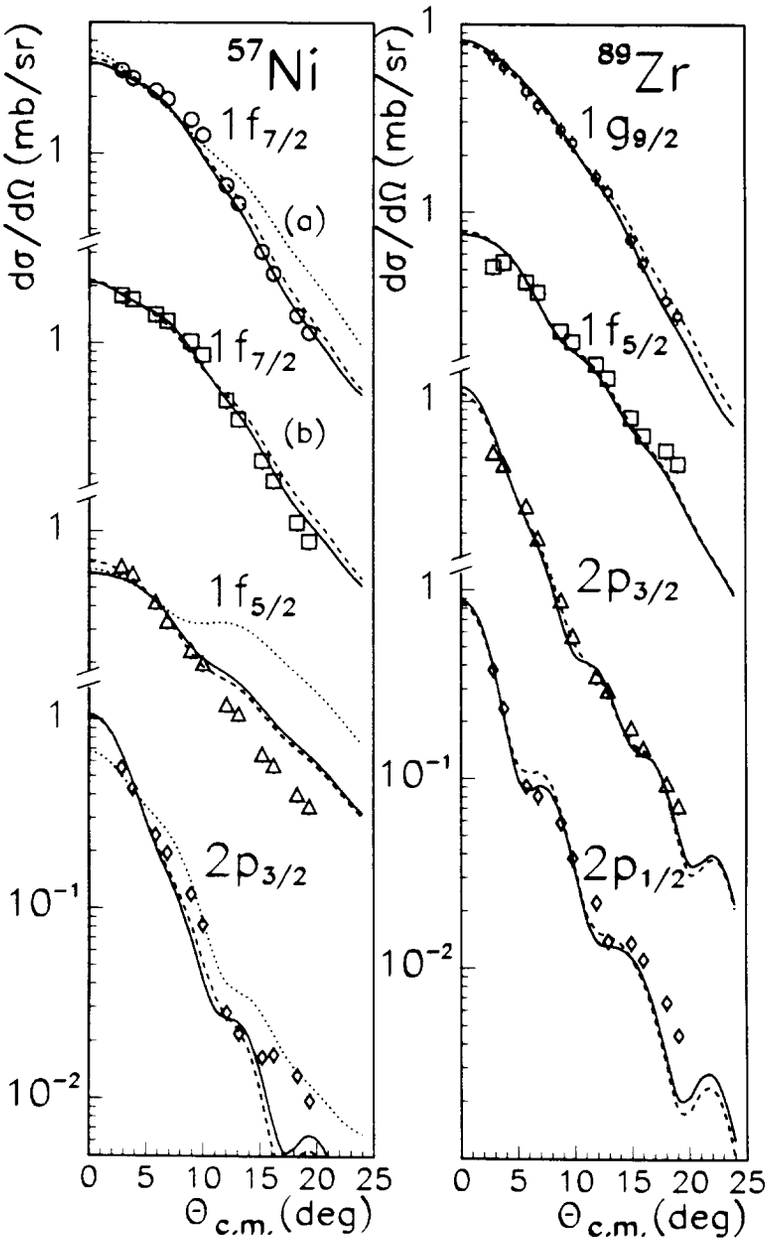
^{57}Ni
$1f_{7/2}$
(a)
$1f_{7/2}$
(b)
$1f_{5/2}$
$2p_{3/2}$
^{89}Zr
$1g_{9/2}$
$1f_{5/2}$
$2p_{3/2}$
$2p_{1/2}$
dσ/dΩ (mb/sr)
$\Theta_{c.m.}$ (deg)
0 5 10 15 20 25
1
10^{-1}
10^{-2}

Fig. 4

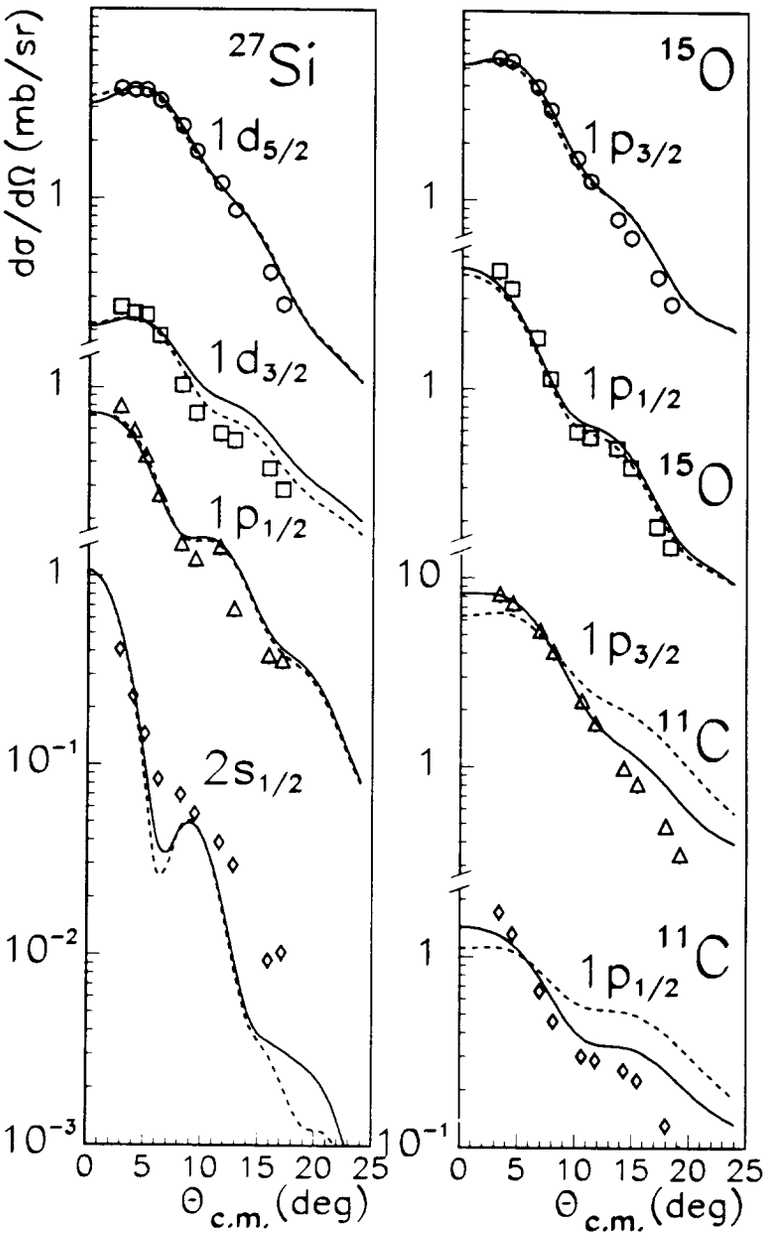
dσ/dΩ (mb/sr)
27Si
1d5/2
1d3/2
1p1/2
2s1/2
15O
1p3/2
1p1/2
15O
1p3/2
11C
1p1/2
11C
Θc.m. (deg)
Θc.m. (deg)

Fig. 5

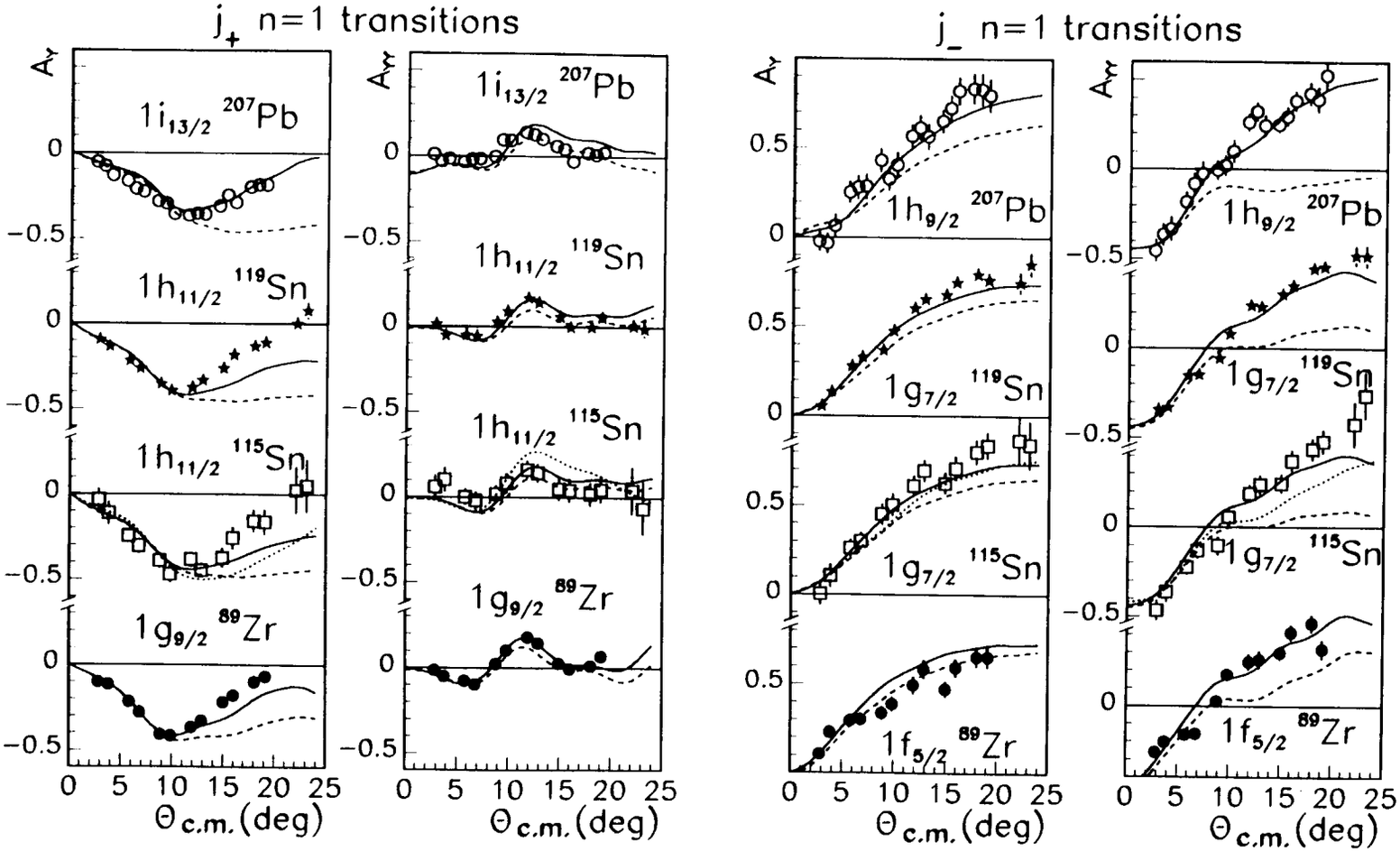
j+ n=1 transitions
j- n=1 transitions
1i13/2 207Pb
1h11/2 119Sn
1h11/2 115Sn
1g9/2 89Zr
1h9/2 207Pb
1g7/2 119Sn
1g7/2 115Sn
1f5/2 89Zr
Ay
Θc.m.(deg)

Fig. 6

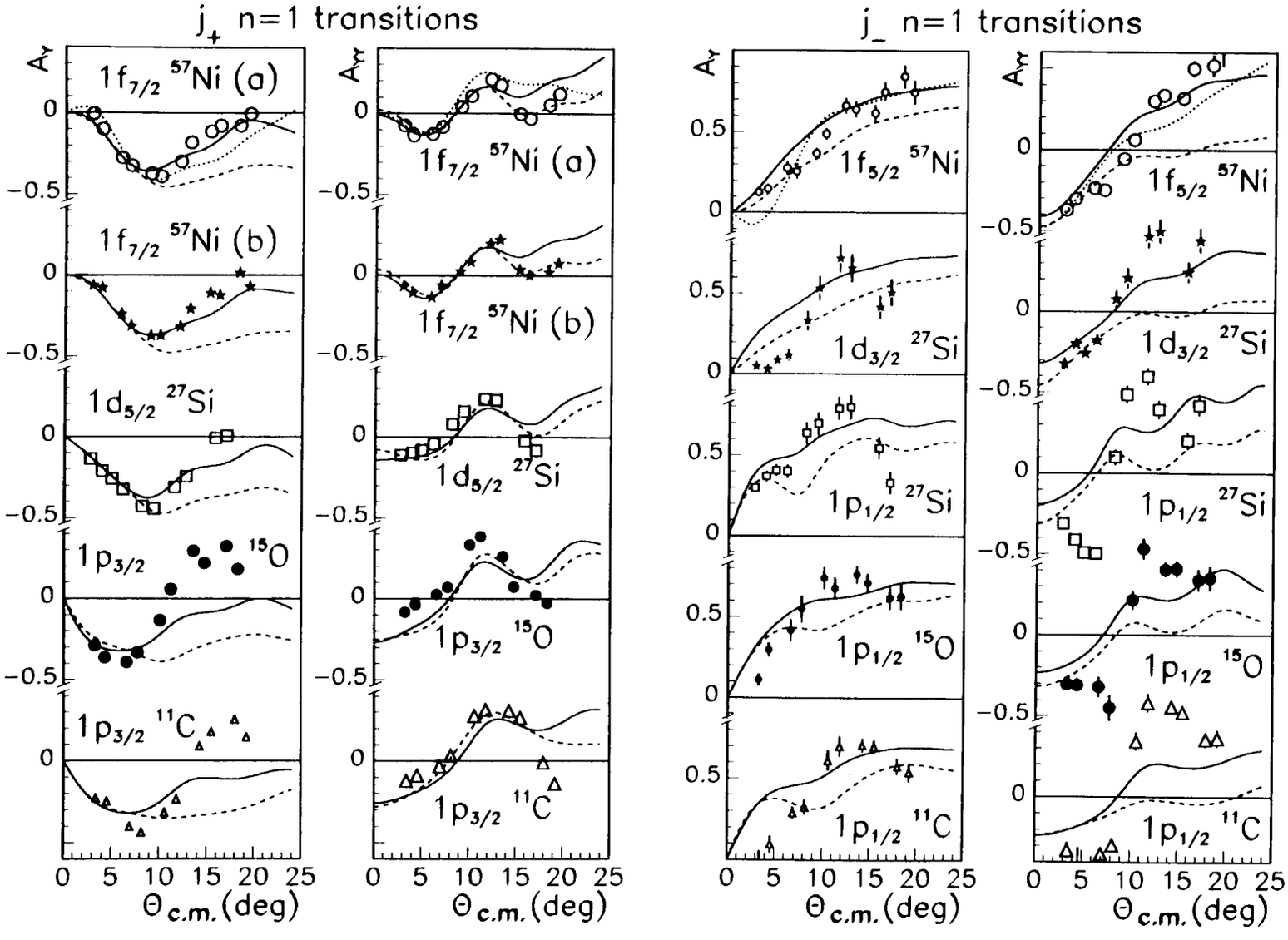
j+ n=1 transitions
j- n=1 transitions
Ayy
1f7/2 57Ni (a)
1f7/2 57Ni (b)
1d5/2 27Si
1p3/2 15O
1p3/2 11C
1f5/2 57Ni
1d3/2 27Si
1p1/2 27Si
1p1/2 15O
1p1/2 11C
0 5 10 15 20 25
Θc.m.(deg)

Fig. 7

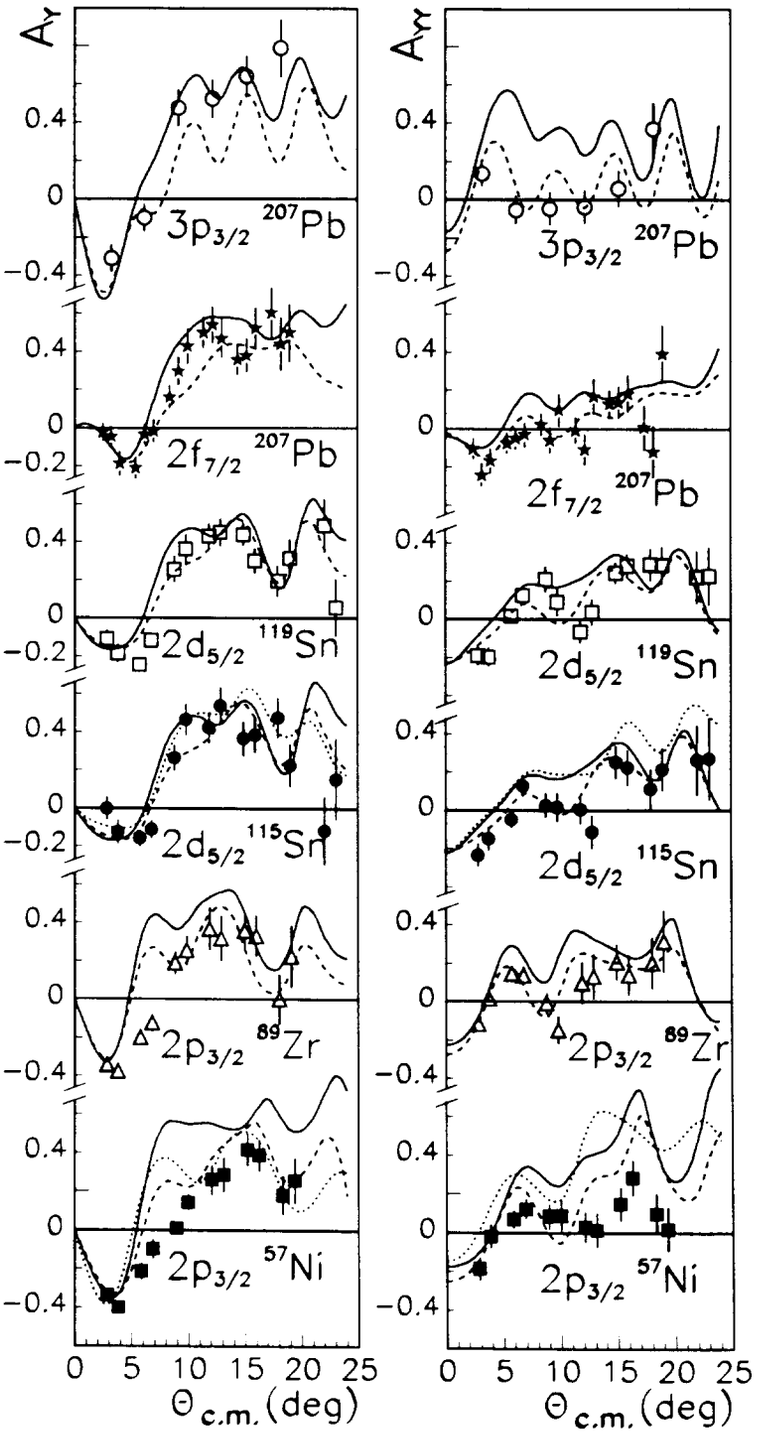
A_Y
A_{YY}
0.4
0
−0.4
−0.2
$3p_{3/2}$ ^{207}Pb
$2f_{7/2}$ ^{207}Pb
$2d_{5/2}$ ^{119}Sn
$2d_{5/2}$ ^{115}Sn
$2p_{3/2}$ ^{89}Zr
$2p_{3/2}$ ^{57}Ni
0 5 10 15 20 25
$\Theta_{c.m.}$ (deg)

Fig. 8

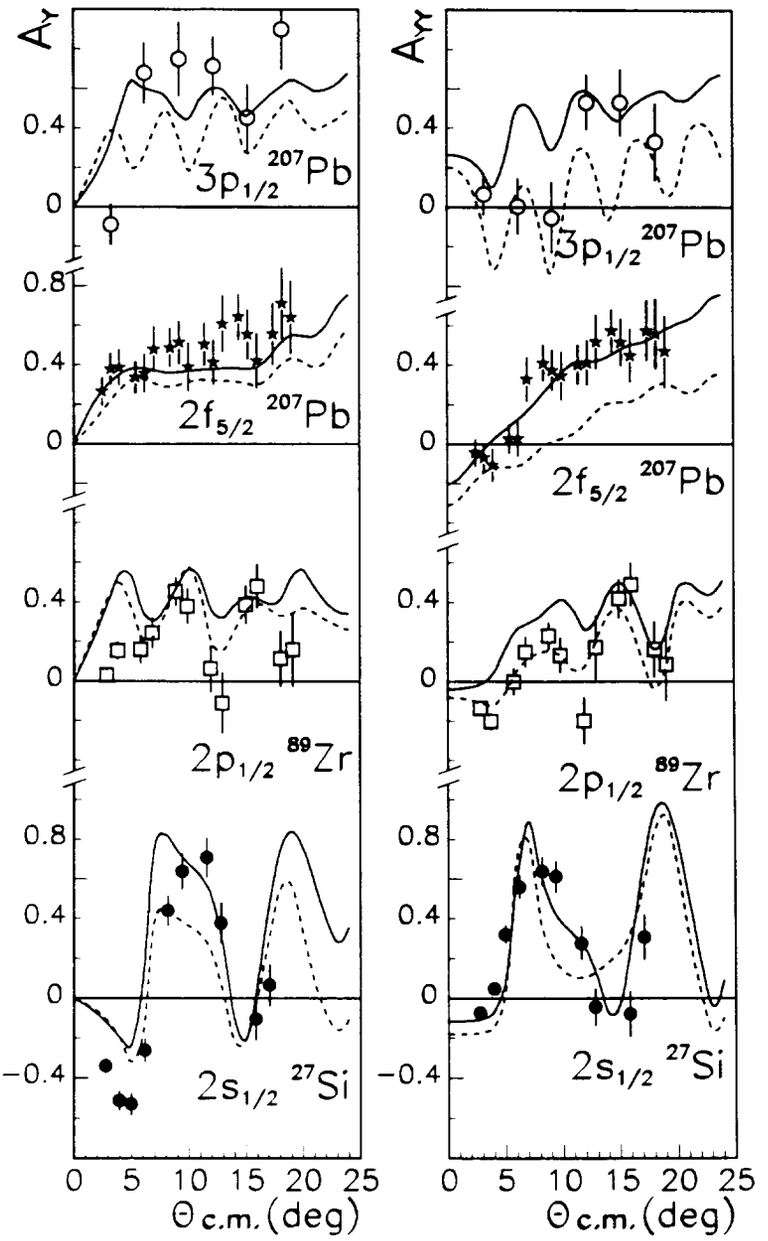
A_Y
A_{YY}
0.4
0
0.8
$3p_{1/2}$ ^{207}Pb
$2f_{5/2}$ ^{207}Pb
$2p_{1/2}$ ^{89}Zr
$2s_{1/2}$ ^{27}Si
−0.4
0 5 10 15 20 25
Θ c.m. (deg)

Fig. 9

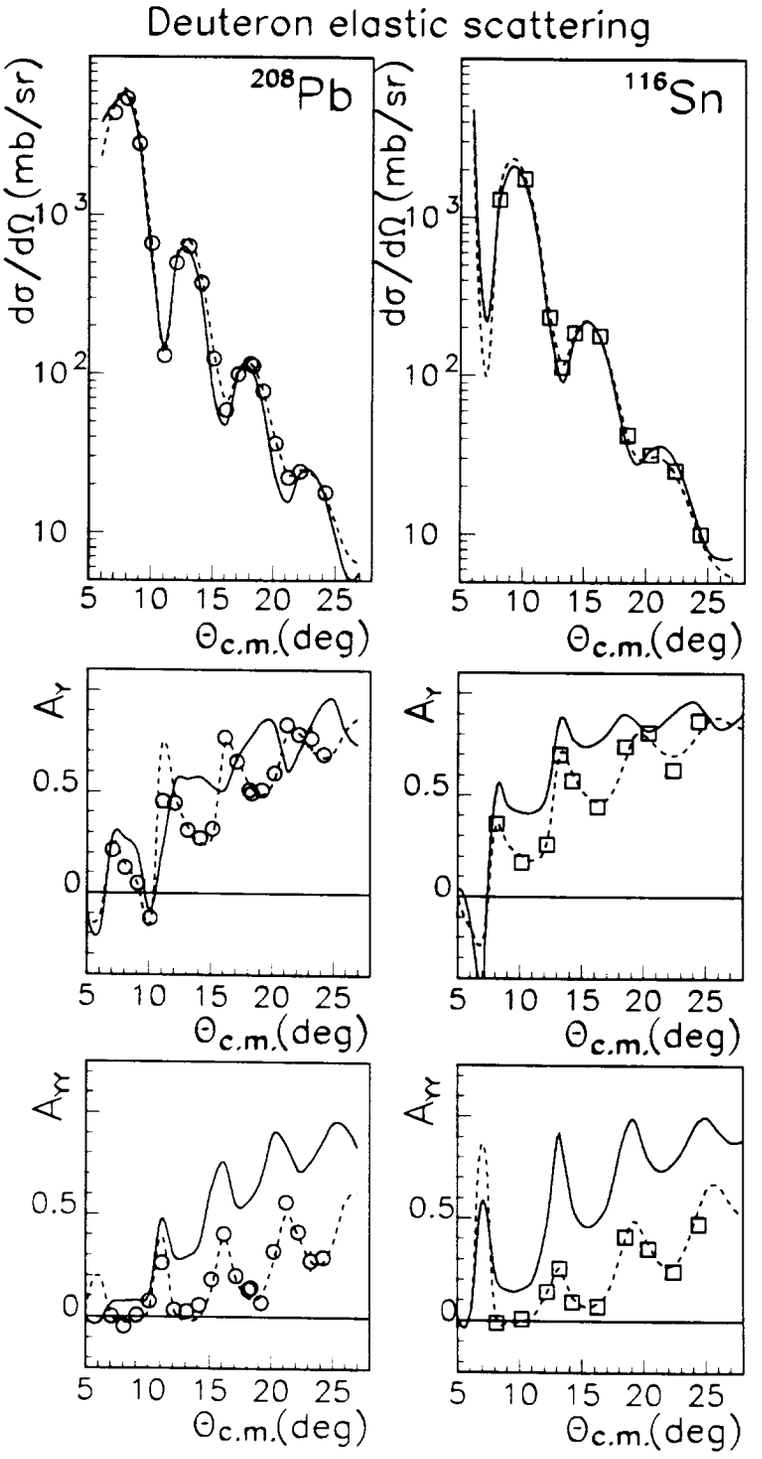
Deuteron elastic scattering
208Pb
116Sn
dσ/dΩ (mb/sr)
10³
10²
10
Θc.m.(deg)
5 10 15 20 25
Ay
Ayy
0.5
0

Fig. 10

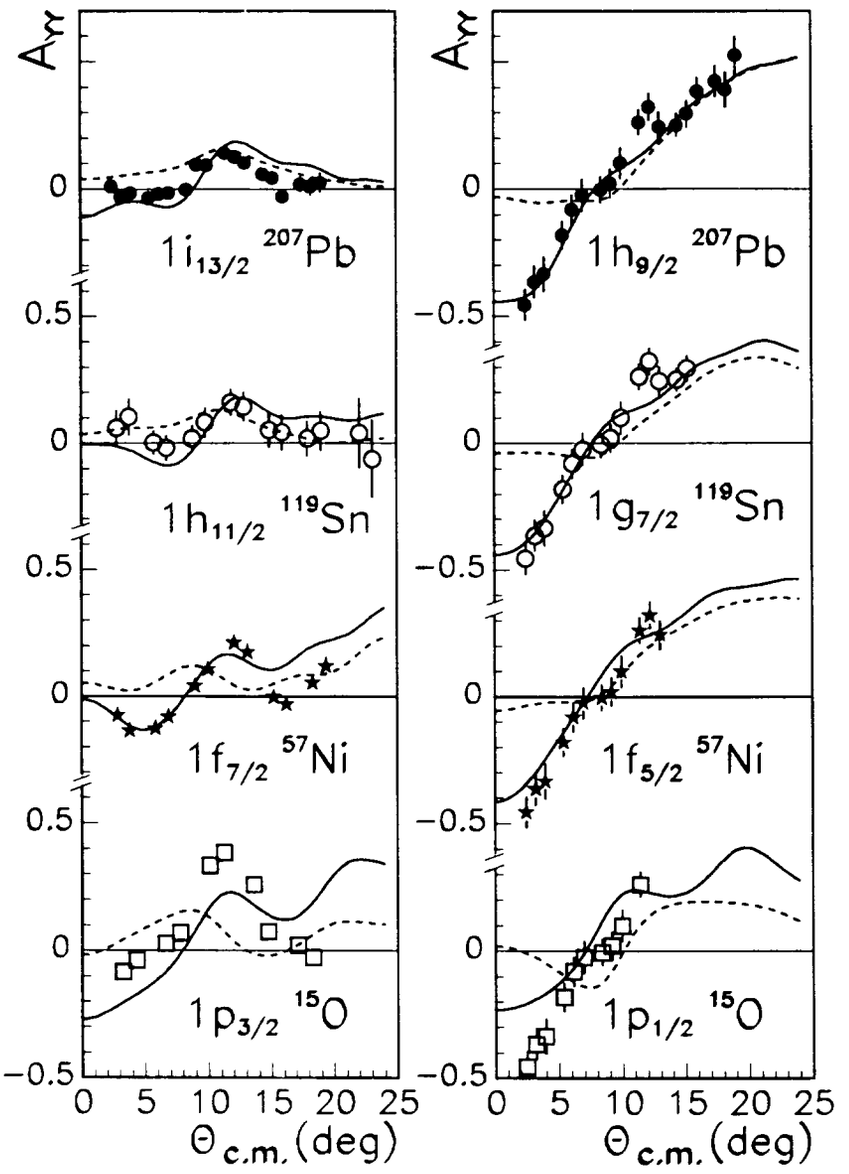
A_{yy}
0
0.5
−0.5
$1i_{13/2}$ ^{207}Pb
$1h_{11/2}$ ^{119}Sn
$1f_{7/2}$ ^{57}Ni
$1p_{3/2}$ ^{15}O
$1h_{9/2}$ ^{207}Pb
$1g_{7/2}$ ^{119}Sn
$1f_{5/2}$ ^{57}Ni
$1p_{1/2}$ ^{15}O
0 5 10 15 20 25
$\Theta_{c.m.}$ (deg)

Fig. 11